

Centrifugal generation and manipulation of droplet emulsions

Stefan Haeberle · Roland Zengerle · Jens Ducrée

Received: 16 February 2006 / Accepted: 8 June 2006 / Published online: 12 July 2006
© Springer-Verlag 2006

Abstract This work for the first time describes a centrifugal technique for the production and manipulation of highly monodisperse water droplets (CV of droplet diameter below 2%) immersed in a continuous flow of immiscible oil. Within a given working range, droplet volumes (5–22 nL) and their mutual spacing is governed by the channel geometry and the frequency of rotation. Different regimes of liquid–liquid flows are presented. We also demonstrate capabilities like droplet splitting and sedimentation as well as the production of two colored droplets, thus setting the stage for a novel centrifugal platform for multiphase flows.

1 Introduction

Emulsions are thermodynamically unstable multiphase systems consisting of at least two immiscible liquids. Within an emulsion, small droplets of the internal or discontinuous phase are dispersed throughout the other, so-called external or continuous phase. Despite their principal instability, emulsions can be set in

metastable state where the droplets retain their integrity for extended periods of time if their phase interface is supported by surfactants. The production of emulsions constitutes an essential part of a large number of process engineering applications within the production chain of food, cosmetics, or pharmaceuticals. With the advent of microfluidic systems, droplet emulsions are also considered a promising candidate for analytical systems. As the size of the droplets often plays a vital role in the application, it is essential to accurately control the droplet dimensions and volume fractions within the multiphase system.

Standard processes use high shear forces to generate droplets, e.g. by rotor-stator, ultrasonic or high-pressure homogenizing systems. However, as the fundamental droplet formation mechanism is of statistical nature, these methods lead to broad droplet-size distributions. Another disadvantage of these conventional production techniques is the parasitic heat induced into the multiphase system which may, for instance, interfere with sensible pharmaceutical substances.

Droplets can also be generated by the surface tension controlled break-off issued from tiny orifices. In this case the droplet size is tightly correlated to the cross section of the orifice. Ideally, a constant flow rate thus allows to produce a highly monodisperse train of droplets. Following this scheme, several microfluidic methods for the production of droplets have been presented (Thorsen et al. 2001; Ganan-Calvo and Gordillo 2001; Anna et al. 2003; Sugiura et al. 2001; Link et al. 2004; Hessel et al. 2002). The controlled manipulation of droplets in the confining rigid boundaries of microchannels can also be applied for additional unit operations in droplet processing like splitting, merging, or separation. We here investigate

S. Haeberle (✉) · R. Zengerle · J. Ducrée
Laboratory for MEMS Applications,
Department of Microsystems Engineering (IMTEK),
University of Freiburg, Georges-Koehler-Allee 106,
79110 Freiburg, Germany
e-mail: haeberle@imtek.de

R. Zengerle · J. Ducrée
HSG-IMIT—Institute for Micromachining and Information
Technology, Wilhelm-Schickard-Straße 10,
78052 Villingen-Schwenningen, Germany

the formation and the controlled manipulation of liquid–liquid flows on our recently introduced centrifugal microprocess engineering platform (Haeberle et al. 2005a, b, c; Ducrée et al. 2004, 2006).

This paper is structured as follows. Section 2 describes the physics of centrifugal droplet generation and its difference to pressure driven mechanisms. In Sect. 3, the mechanism of droplet formation in a centrifugal driven flow-focusing structure is presented. Section 4 describes the different types of multiphase flows realized with this approach and important unit operations for droplet processing like splitting of droplets, droplet sedimentation, and the production of biphasic droplets.

2 Physics of centrifugal droplet generation

In the here presented centrifugal multiphase flow platform (Haeberle et al. 2005d), liquid propulsion results from the centrifugal pseudoforce generated by the rotary motion of a microfluidic channel network. Considering a *static* case of a liquid plug resting within the rotating frame of reference, an equivalent pressure can be derived at the radial outer end of the plug, scaling with the square of the rotational frequency ω (Brenner et al. 2005). However, the hydrodynamics within a centrifugal liquid *flow* deviates significantly from pressure driven flows. In the following, two differences are highlighted that are of particular importance for multiphase liquid flows.

First, the centrifugal force represents a body force acting on each fluid volume element while the propulsion by an external pressure difference is transmitted by the surface. This, for instance, impedes the centrifugal pumping of gases due to their low density while enabling the active “falling” of particles or droplets throughout a carrier liquid of lower density.

Secondly, the centrifugally induced “artificial gravity” linearly increases with the radial distance from the center, leading to an internal pressure distribution in a liquid flow which settles below the (atmospheric) pressure at the open inlet and outlet of the channel (Kim and Kwon 2006). This unique pressure distribution eases the requirements on the sealing of the microchannels, allowing very high flow rates and throughputs (Haeberle et al. 2005).

A characteristic distribution of the relative pressure along the center of a microchannel (length 3 cm, width 300 μm , height 200 μm , radial position of the inlet 2 cm) for a pressure as well as a centrifugal driven flow is depicted in Fig. 1 (CFD-ACE+, ESI CFD, Inc., Huntsville, AL, USA). The volumetric flow rate of

172 $\mu\text{L s}^{-1}$ of the simulated centrifugal flow for $\omega = 377 \text{ rad s}^{-1}$ is imposed as an inlet boundary condition in the pressure driven flow. The two pressure distributions display a strikingly different character: the relative pressure distribution of the pressure driven flow exhibits a maximum at the inlet of approximately 1 bar. However, the relative pressure of the centrifugal flow coincides with the ambient pressure at the “open” inlet and outlet of the channel, respectively. In between, the relative pressure becomes negative (neglecting entrance effects).

These distinct centrifugal hydrodynamic conditions imply characteristic deviations regarding the droplet generation principles compared to a pressure-driven flow. For example, the issuing of gas bubbles into a continuous liquid flow at a flow-focusing junction has been intensively investigated in pressure driven systems (Garstecki et al. 2004, 2005). Evidently, this approach cannot directly be implemented on the centrifugal platform since the buoyancy prohibits a concurrent centrifugal propulsion of the gas phase in the continuous liquid phase, thus requiring an inde-

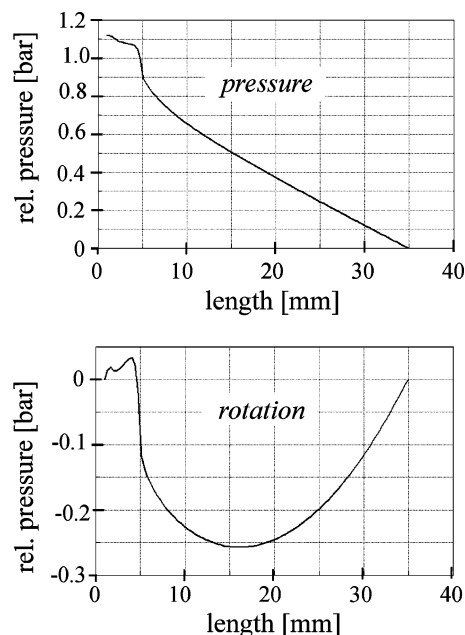


Fig. 1 Distributions of the relative pressures along the center of a 3-cm long microchannel exhibiting a cross section of 300 $\mu\text{m} \times 200 \mu\text{m}$ for a pressure driven (*top*) and centrifugal flow (*bottom*) at a flow rate of 172 $\mu\text{L s}^{-1}$ for both cases. An almost linear decay of the relative pressure with a maximum of ~ 1 bar at the inlet is observed in the pressure driven flow (*top*). The centrifugal flow (*bottom*) is confined by a vanishing relative pressure at the inlet and outlet, respectively. In between, the hydrodynamic pressure falls below the ambient pressure (discarding the slight increase at the very entrance). The radial position of the inlet was set to 2 cm in the centrifugal flow model

pendent pressure source for the gas on the centrifugal platform (Haerberle et al. 2006).

The basic impact parameters governing the centrifugally induced droplet formation process at the junction of a flow-focusing structure (Anna et al. 2003) under rotation are depicted in Fig. 2. The two pulling forces, namely the centrifugal force (density) F_ω and the hydrodynamic drag F_d of the sheath flows ϕ_o expel the water flow out of the central channel. The break-off of the water droplets is stimulated by the geometric constriction right after the junction as well as the inertia associated with the transversal component of the oil flows (F_i).

The centrifugal force depends on the density difference of the two phases, the radial position of the nozzle and the square of the rotational frequency ω . The magnitude of the constricting oil flow depends on the radial position, the radial height, and the hydrodynamic resistance of the oil guiding channels as well as the square of ω .

The interfacial tension force F_σ of the emerging liquid bridge between the droplet and the central inlet channel is the counterforce opposing the droplet break-off. F_σ scales with the interfacial tension σ between the water and oil phase as well as the (minimum) circumference of the bridge indicated by the white line in Fig. 2 (assuming no bending along the channel height). During the droplet formation process, the overall interfacial area of the plug exposed to the focusing oil flow expands and thus also the impact of the hydrodynamic drag F_d and inertial forces F_i of the constricting oil flows ϕ_o . F_i tends to squeeze the interface back into the issuing nozzle until the plug exceeds a critical dimension. As soon as the plug is long enough, however, F_i restricts the circumference of the bridge and therefore supports the droplet break-off.

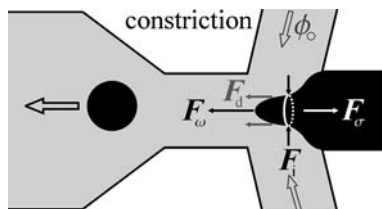


Fig. 2 The basic channel design and hydrodynamic influence parameters on the droplet formation process. The centrifugal force (density) $F_\omega = \rho\omega^2$ and the drag F_d of the sheath flows ϕ_o represent the pulling forces supporting droplet formation. The emerging droplet is squeezed by the inertia induced by the transversal component of the sheath flow (F_i). The surface tension counterforce F_σ depends on the circumference of the meniscus (white interface) and prevents the droplet break-off until a critical mass is reached

The opposing pulling and interfacial force depend on the transient shape and volume of the evolving liquid plug and thus the droplet break-off takes place as soon as the plug exceeds a critical mass for a given (minimum) circumference of the liquid bridge. Since both the flow velocity of the plug as well as the critical mass depend on the frequency of rotation ω , the droplet generation frequency f as well as the droplet size (diameter d , projected surface area A) can be manipulated by changing ω . The droplet generation process on the centrifugal multiphase platform can therefore be described as a dripping nozzle in a frequency controlled artificial gravity field $z\omega^2$, assisted by symmetric outer strangulating and sweeping oil flows ϕ_o . The coordinate z denotes the radial position from the center of rotation, amounting to about 3 cm in our system.

Following these hydrodynamic considerations, the diameter of the droplets d should shrink towards decreasing cross section of the junction as well as towards increasing oil flow rate ϕ_o and centrifugal body force F_ω . Also the droplet generation frequency f is supposed to increase with ϕ_o and F_ω . Since both, ϕ_o and F_ω , scale with ω^2 , the rotational frequency ω acts as a dynamically adjustable setscrew for an online control of the droplet size d and droplet formation frequency f .

A dimensionless number that expresses the scaling of effects related to the viscous shear stress with respect to the interfacial tension (Link et al. 2004; Joannicot and Ajdari 2005) is the capillary number

$$Ca = \frac{\eta u}{\sigma} \tag{1}$$

with the viscosity of the continuous phase η , the interfacial tension between the two phases σ , and the velocity of the dispersed phase out of the channel into the junction area u (Tan et al. 2004).

Different modes of droplet formation are observed for different capillary numbers, Ca . For low Ca (< 1), droplets are formed directly at the junction of the structure. This droplet formation mechanism is referred to as the “dripping” regime (Utada et al. 2005). Towards large Ca , the “jetting regime” is entered where axially extended plugs of the dispersed liquid are injected into the continuous phase (Cramer et al. 2004). These jets are poorly stable and tend to break-off into droplets upon transient fluctuations within the jet (Rayleigh instability, Lord Rayleigh 1878). Due to the statistical nature of such a break-off, a broad droplet-size distribution is observed (Utada et al. 2005). As this work aims at the production of highly

monodisperse droplet trains, the “dripping” mode is the method of choice.

However, the capillary number Ca does not take directly into account the special conditions in the centrifugal “artificial gravity” field $z\omega^2$ as well as the dimensions of the orifice at which the droplet breaks up into the continuous phase. The impact of the artificial gravity on the droplet formation is accounted by the Bond number

$$Bo = \frac{a\rho_d L^2}{\sigma} = \frac{z\omega^2 \rho_d L^2}{\sigma} \quad (2)$$

representing the ratio of centrifugal and interfacial effects on the droplet. ρ_d describes the density difference between the two phases and L the characteristic length scale, i.e. L^2 the cross section of the issuing nozzle.

With typical angular frequencies of $\omega = 2\pi\nu = 100 \text{ rad s}^{-1}$, common values of the centrifugally induced artificial gravity a range in the order of several 100 m s^{-2} with the gravitational acceleration $g = 9.81 \text{ m s}^{-2}$, i.e., a 10-fold increase of g (Eq. 2). Towards elevated frequencies ω , Bo increases and the impact of the surface tension reduces to promote the centrifugally induced “drawing” of jets from the nozzle. For a given set of liquids, dripping is thus linked to small capillary numbers $Ca \sim u \sim \omega^2 L^2$ (Ducree et al. 2005) as well as small Bond numbers $Bo \sim aL^2 \sim \omega^2 L^2$. As both, Ca as well as Bo , scale with $\omega^2 L^2$, the dripping regime is favored by small cross sections L^2 of the issuing nozzles as well as small rotational frequencies ω .

Nevertheless, the capillary number Ca cannot be regarded as the primary control parameter for the droplet volume V_d since it does not represent the exact details of the droplet formation mechanism in a

microfluidic flow focusing geometry. The droplet volume V_d in pressure driven flow focusing devices (FFD) has been described as a function of the flow rate Φ_o and the viscosity η of the continuous as well as the pressure p within the dispersed phase at the junction ($V_d \propto p / \Phi_o \eta$) (Garstecki et al. 2004, 2005).

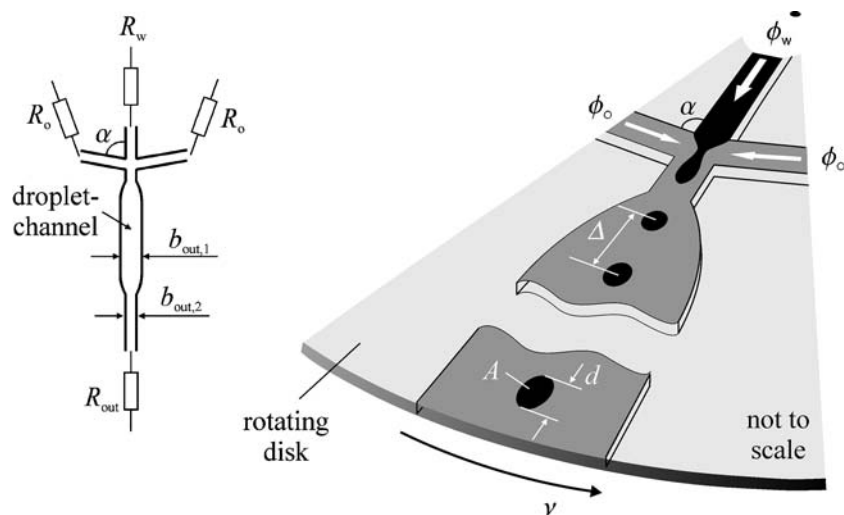
In the centrifugal driven FFD, the continuous flow rate Φ_o as well as the pressure inside the dispersed phase p scale with ω^2 and thus V_d ought to be independent of the frequency of rotation ω . However, our experimental investigations will reveal a change of the droplet diameter with ω . We consider the additional centrifugal volume force F_ω resulting in a net force pulling the (more dense) dispersed phase out of the central channel as the main reason for that dependence, thus disclosing the different hydrodynamic nature of the droplet formation mechanisms in centrifugal and pressure driven systems.

3 Centrifugal emulsification

3.1 Channel design and system setup

The channel layout exhibits an inlet for the dispersed phase Φ_w which is enclosed at an angle α by two outer “sheath” flows Φ_o (Fig. 3). Downstream the central junction, the dispersed phase Φ_w is guided by the sheath flows into the common channel carrying the emulsion within a given working range of flow conditions. Subsequently, the multiphase flow is driven along the droplet channel for further processing or characterization. The influence of the channel network on the flow rates in the inlet and outlet channels is quantified by their individual hydrodynamic resistances R_o , R_w of the inlet channels and the outlet channel R_{out} .

Fig. 3 Main geometrical parameters of the droplet generation structure and the produced droplet train. The dispersed phase is contacted from both sides with the continuous phase at the junction of a flow-focusing structure



The flow-focusing structure has been adapted to the needs of the centrifugal microfluidic approach. Therefore, the entire channel layout is arranged symmetrical to the radial droplet channel and placed on a disk-shaped module rotating at a frequency ω about the center of the disk. The characteristics of the produced emulsion, i.e., the droplet cross section A , the droplet diameter d , and the drop-to-drop spacing Δ , are measured optically (Grumann et al. 2005). A , d , and Δ can be influenced by the design parameters, mostly the flow resistances R_o , R_w , and R_{out} as well as the frequency of rotation ω .

All microfluidic channel structures within this paper have been fabricated by high-precision milling into a cyclo-olefin copolymer (COC) substrate with a diameter of 115 mm and a thickness of 2 mm. The channels were sealed by another transparent copolymer foil, using a thermal diffusion bonding process. The contact angles of the used substances with the untreated polymer surface are listed in Table 1.

The complete setup comprises the microstructured polymer disk featuring the flow-focusing microchannels and rotating reservoirs that are mounted on top of the disk (Haerberle et al. 2005a). These reservoirs enable either the storage of a certain liquid volume on the rotating module (several mL) or the continuous injection of additional liquid during rotation. The collection of the multiphase flow after processing can also be realized in a batch-like fashion using onboard reservoirs rotating with the disk or in a continuous fashion by ejecting the liquid onto a stationary drainage ring.

Regarding the device, the main benefit of the centrifugal technology is the modular setup consisting of a robust actuation unit, e.g., a conventional centrifuge, and a passive rotating module without moving parts to process the liquids. The centrifugal propulsion of flow and thus the centrifugally stimulated break-off process then results from the pulse-free spinning motion of the rotor which is stabilized by its own angular momentum. Compared to conventionally pumped systems, the centrifugal principle tends to dampen high-frequency pressure perturbations by its inertial momentum, thus leading to an improved reproducibility of the break-off process.

Table 1 Main rheological properties of water and sunflower oil. Viscosity η , contact angle θ measured on COC, mass density ρ , and the interfacial tension between the two phases σ

	η (mPa s)	θ (°)	ρ (g cm ⁻³)	σ (mN m ⁻¹)
Water	1.09	82.7	1.005	28.33 (Cramer et al. 2004)
Sunflower oil	62.2	10.3	0.909	

3.2 Multiphase system

We investigate a suspension of DI water droplets in sunflower oil (W/O emulsion). The water is colored by 2 vol% ink to enhance the contrast of captured images. No additional surfactants have been added to the continuous phase to stabilize the emulsion since they reduce the interfacial tension and consequently also the required energy to form a droplet by shear stress. Therefore, the system without surfactant has the highest demand on the microfluidic structure in order to form a droplet and serves as a model system. Table 1 shows the properties of the water (W) and the oil (O) phase, respectively. The contact angle has been measured on a planar COC surface.

3.3 Droplet formation in the centrifugal field

Droplets are generated at the junction of the flow-focusing structure where two outer oil flows and an enclosed water column are contacted and then driven through the radial droplet channel. The stroboscopic picture sequence displayed in Fig. 4 shows the droplet formation process under rotation at this part of the structure (Grumann et al. 2005).

Oil exhibits superior wetting properties, i.e., a smaller contact angle θ within the microchannels made of COC (Table 1). Thus, the water plug has to be actively “pulled” out of the central channel by the centrifugal force F_ω , i.e., a critical bond number Bo (Eq. 2) has to be surpassed by increasing the rotational frequency ω . To avoid jetting, the flow velocity u of the dispersed phase out of the central channel into the growing droplet has to be throttled by introducing an elevated hydrodynamic resistance of the central channel R_w . As mentioned in Sect. 1, the throttling reduces the capillary number Ca (Eq. 1) in order to support the desired dripping.

Following the sequence in Fig. 4, the water plug moves towards the center of the focusing structure. With increasing length of the plug, its mass and the effective surface shaped by the interplay of the oil flows and the surface tension grows. As soon as the strangulation by this focusing arrangement and the “artificial gravity” of the centrifugal field on the growing droplet overcomes the surface tension, a droplet is formed and carried away by the ambient oil flow.

4 Generation and manipulation of multiphase flows

As described in the previous section, the droplet formation process can be controlled by the flow condi-

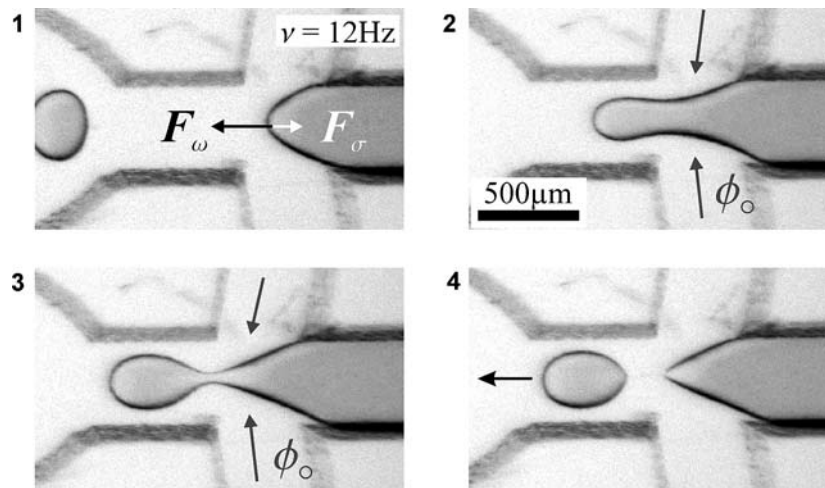


Fig. 4 Stroboscopic sequence of four pictures (1–4), showing the droplet formation process under the impact of the centrifugal field. At the rotational frequency of 12 Hz, an equivalent gravitation of 18g affects the liquids at the radial position of the junction. The ink-colored water substream breaks off to form

a droplet at the junction of the flow-focusing structure. Note that, due to the fast droplet rate and the restricted observation window at one given angular position, the pictures display subsequent stages of the formation process for different droplets

tions at the junction, i.e., mainly by the flow velocities and their respective ratios. The flow velocities are statically defined by the channel resistances R_o , R_w , and R_{out} and they can dynamically be adjusted by changing the angular frequency $\omega = 2\pi\nu$ (Haeberle et al. 2005b).

4.1 Droplet trains and segmented flow

In this section, we present three different structures for the production of water droplets in a continuous oil-flow (W/O emulsions). Additionally, their main characteristics, namely the distribution of the droplet diameters d , the spacing between the droplets Δ , and the droplet production rate f are studied. The droplet spacing Δ is connected to the ratio between the droplet generation frequency and the flow rate within the outlet channel, i.e. the ability of the system to remove the generated droplets from the junction area.

Depending on the droplet size, the generated multiphase flows in Fig. 5 can be categorized into three different types:

1. *Isolated droplet trains*: The diameter of water droplets falls short of the channel height. Thus, the droplets retain a spherical shape minimizing the surface tension.
2. *Squeezed droplet trains*: The (relaxed) diameter of the water droplets exceeds the channel height. This mode could be used to produce, e.g. nonspherical microparticles (Dendukuri et al. 2005).

3. *Segmented flow*: The (relaxed) diameter of the water droplets is larger than the height and the width of the channel. This mode is of interest for analytical applications (Song et al. 2003; Shestopalov et al. 2004; Roach et al. 2005).

The channel structures for the production of these types of emulsions are all based on the earlier presented flow-focusing principle (Fig. 3). Only the hydrodynamic resistances of the water R_w and oil R_o channels as well the shape and resistance of the droplet channel R_{out} are adjusted according to Table 2.

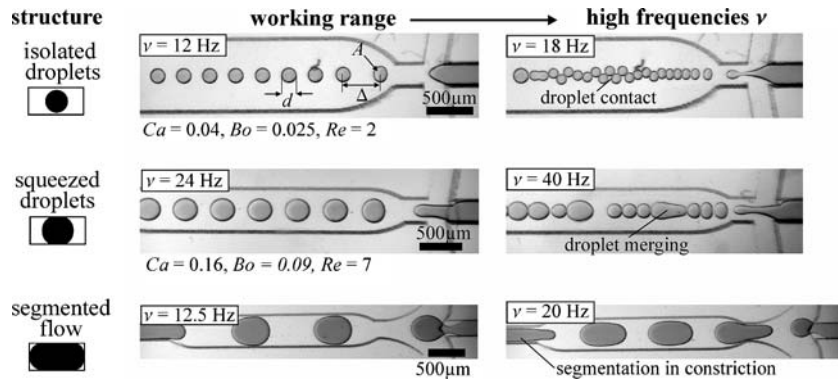
The hydrodynamic resistance of low-aspect-ratio microchannels with a length l , a width w , and a height h is given by

$$R = 12\eta \frac{l}{wh^3} \quad (3)$$

for a liquid with viscosity η (Geschke et al. 2004). In Table 2, the geometrical part $R' = R/12\eta = l/wh^3$ of the fluidic resistance R is listed to focus on the free design parameters of the flow-focusing structure.

Highly monodisperse droplet trains are generated within a certain window of rotational frequencies for all three emulsification structures (Fig. 5). At low frequencies of rotation, no droplets are formed since the water plug rests in the central channel or even withdraws due to the favored oil-wetting behavior within the channels (low Bond number, Bo). However, above a certain frequency threshold ν_{low} , a water plug pro-

Fig. 5 Spatially separated droplets are generated within the working range. Depending on the geometry of the structure and the rotational frequency, modes of isolated droplets, squeezed droplets as well as segmented flows can be realized within the droplet channel



trudes into the junction region and breaks up into equally sized droplets within the working range of the structure.

The isolated structure produces the smallest droplets indicating the magnitude of the strangulating oil flow as one major parameter influencing the droplet size. The hydrodynamic resistance of the oil and the outlet channel are small in that design thus scaling up the oil flow through the flow-focusing structure (the cross section of the central channel is the same for all three structures: $\sim 340 \times 110 \mu\text{m}^2$).

In Fig. 5, also the capillary numbers, Ca , are given for two structures within the working range. The values for Ca have been calculated using Eq. 1, identifying the droplet velocity in the droplet channel with the mean velocity of the dispersed phase into the junction area u . The low values of Ca indicate that the upper frequency limit ν_{high} of working range where separate droplets can still be discerned is not determined by the transition of the droplet generation effect from dripping to jetting (which occurs at even higher frequencies of rotation, see Fig. 6). Instead, the limitation is associated with the contact ($\Delta = d$) and merging of the initially separate droplets which are not removed fast enough from the junction area by the continuous oil flow.

Two parameters, the characteristic droplet area A and the droplet spacing Δ , can directly be derived from

the stroboscopic grayscale pictures. An image processing algorithm has been used to automatically determine A by changing the picture contrast and searching for the outline of the ink-darkened water droplet. The diameter of the droplets d is calculated by assuming round droplets.

This is certainly an approximation since the droplets are squeezed to an unknown extent between the upper and lower wall of the channel (depth $\sim 200 \mu\text{m}$). Consequently, also the droplet volume can only be estimated by multiplying the characteristic area A with the measured channel depth.

Figure 7 shows the calculated droplet diameter d as well as the droplet spacing Δ of the squeezed and isolated droplets structures over the frequency of rotation ν . The squeezed-droplet structure displays a wider working range since the flow velocity within the droplet channel is higher and thus the droplets are removed faster from the junction to avoid contacting of the issued droplets. Towards increasing frequencies of rotation, the droplet generation rate grows while their size shrinks (Fig. 7). Above the upper limit of the working range ν_{high} , the droplets get in contact or even merge. This indicates the thermodynamic instability of the surfactant-free macro-emulsion displaying a droplet diameter in the range of several hundred micrometers (Windhab et al. 2005).

Table 2 Geometric parameters of the three emulsification structures. The droplet-channel length (25 mm), height (200 μm), and the junction angle ($\alpha = 80^\circ$) are kept constant for all presented channel structures

	Isolated droplets	Squeezed droplets	Segmented flow
$R'_w (10^{12} \text{ m}^{-3})$	150	74	110
$R'_o (10^{12} \text{ m}^{-3})$	0.17	1.3	1.5
$b_{\text{out},1} (\mu\text{m})$	1,048	660	707
$b_{\text{out},2} (\mu\text{m})$	1,048	376	391
Junction	Straight	Straight	Smooth

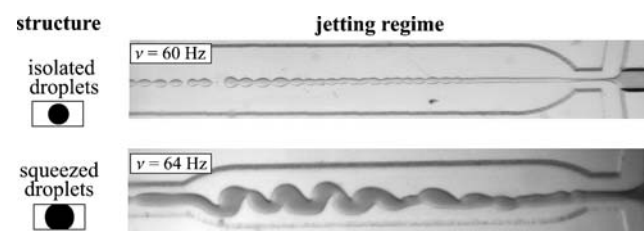


Fig. 6 Multiphase flow patterns within the jetting regime for the isolated (top) and squeezed (bottom) droplet structure at very high frequencies of rotation

The high monodispersity of the droplet trains is depicted in Fig. 8. The figure displays the diameter of 100 droplets produced in the isolated-droplet structure at a rotational frequency of 12 Hz. The mean diameter \bar{d} of 211.33 μm relates to a droplet volume of approx. 7.7 nL. An extremely small coefficient of variation (CV = standard deviation / mean) proves the high reproducible break-off process in the centrifugal flow focusing structure.

Another important parameter that cannot be directly derived from the stroboscopic picture sequences is the droplet generation frequency f . A special mode of operation of the emulsification structures is used to determine f by the number of droplets issued in a fixed time interval Δt . First, the rotational frequency ω is kept below the threshold frequency where no droplets are produced. Afterwards, ω is raised as fast as possible with our centrifuge to the desired value and droplets are ejected at the junction. The time period for the acceleration lasts approximately 0.45 s for the largest frequency step from 10 to 28 Hz since the maximum acceleration of the centrifuge amounts to 40 Hz s^{-1} .

Now, the number of produced droplets $n_{d,t}$ and $n_{d,t+\Delta t}$ of two subsequent stroboscopic pictures can be evaluated (Fig. 9). Since only fully developed droplets are considered, this method leads to a certain discretization error. The delay Δt between two subsequent stroboscopic pictures is set by the known capture frequency of the stroboscopic camera to arrive at

$$f = \frac{n_{d,t+\Delta t} - n_{d,t}}{\Delta t} \quad (4)$$

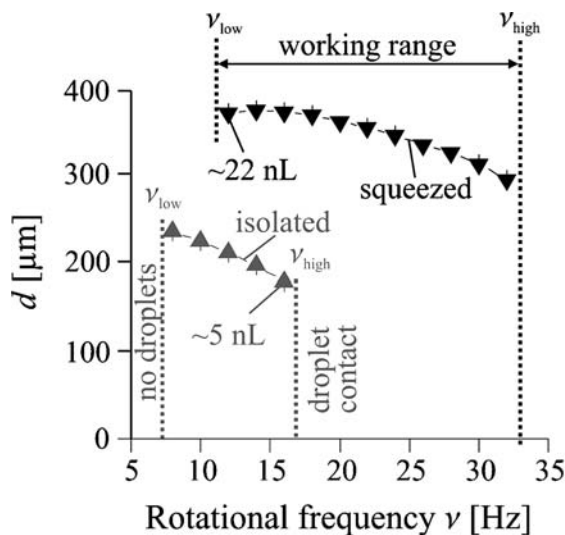


Fig. 7 The droplet diameter d and their mutual spacing Δ as a function of the geometry and the frequency of rotation $\nu = \omega/2\pi$. The increased oil flow due to the smaller hydrodynamic

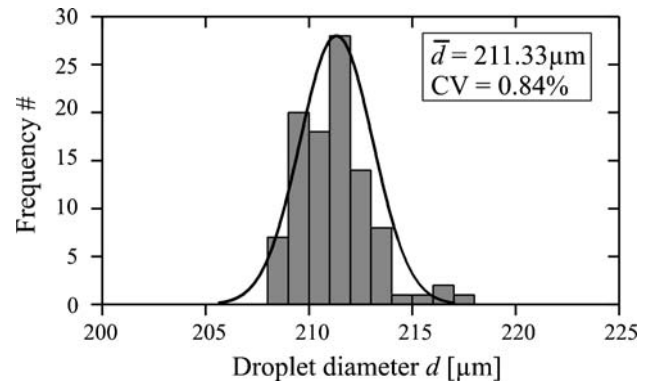
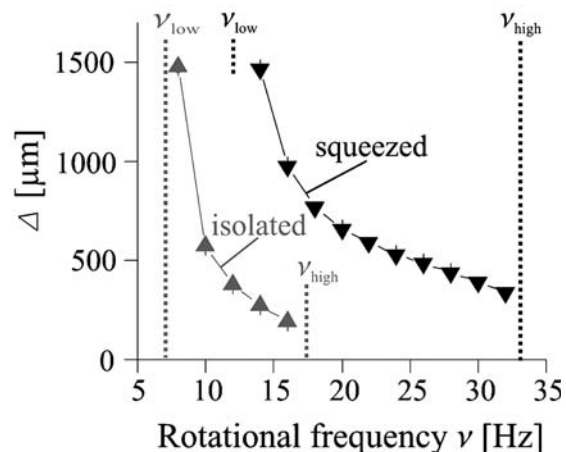


Fig. 8 A representative size distribution for the isolated-droplets structure (see Fig. 5 middle) at 12 Hz shows the high monodispersity (CV = 0.84 % = standard deviation/mean) of the produced emulsions

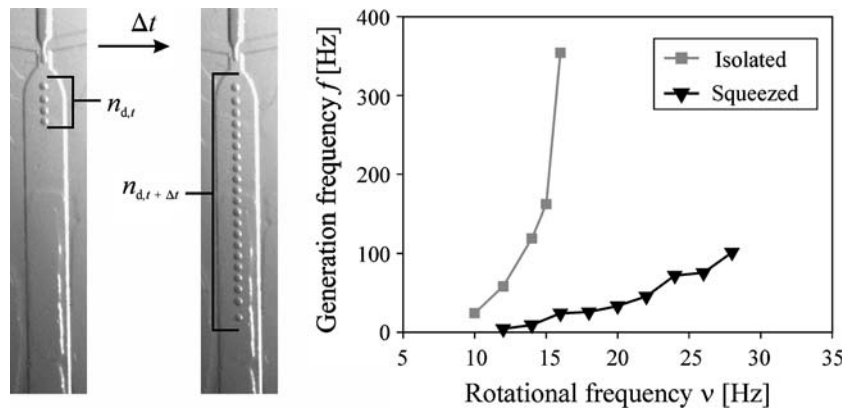
for the droplet rate. The “droplet counting method” is limited by the minimum time delay between two pictures, the maximum display window of the optical setup and the radial velocity of the droplets within the droplet channel. These parameters restrict the possibility to count all produced droplets in the second picture because as soon as the droplet train leaves the display detail, the required information of the number of droplets cannot be determined.

As depicted in Fig. 9, the droplet generation frequency f ranges from several ten up to about 400 droplets per second. The throughput may appreciably be enhanced by operating several channels on one rotational module or even several modules as a vertical



resistances (see Table 2) leads to smaller droplet within the isolated droplets design

Fig. 9 The number of produced droplets is counted in two subsequent pictures (left) to determine the droplet generation frequency f for the isolated and squeezed droplets structures (right)



stack in parallel (Ducrée et al. 2004). Our platform thus allows the controlled production and processing of a small number of droplets as well as a fast production of monodisperse emulsions.

4.2 Droplet splitting

Besides the controlled production of droplets, also their manipulation is important to enable droplet-based fluidic applications. We first study the splitting of a droplet into several subdroplets of defined size. To this end, a second flow-focusing junction on an outer diameter of the droplet channel is used to hydrodynamically induce the splitting of droplets generated further upstream (Fig. 10).

Depending on the frequency of rotation, the droplet is again squeezed at the junction by two lateral oil flows Φ_o . Below a critical frequency, the velocity of these flows and consequently also their constricting impact remains too small, and the droplets are just transiently

squeezed and then relax back to its equilibrium shape right after the junction. Beyond the critical frequency of roughly 21 Hz for the presented channel layout in Fig. 10, the droplet is completely split at the junction, and two spatially separated droplets proceed in the downstream direction. A further increase of the frequency of rotation leads to such a reinforced flow focusing at the junction, even reproducibly stimulating the isolation of a satellite droplet.

4.3 Droplet sedimentation

Processing different immiscible liquids in multiphase flows also implies the simultaneous processing of fluids with different rheological properties in the same system. The emulsification process is also referred to as mixing as it can also be looked at as a first step to homogenize the phase distribution. We here investigate the reverse unmixing or separation process which constitutes an important unit operation within many applications. Our centrifugal platform enables simple separation methods based on density differences of the phases by an accelerated sedimentation in the centrifugal force field.

The ability to selectively control the different phases is shown with a flow-splitting structure (Fig. 11). The multiphase W/O-emulsion flow is split into two outlet channels. Owing to their slightly increased mass density (~1%), the droplets are driven towards the outer wall within the guide channel. After the bending, the radially outwards pointing centrifugal force continues pressing them against the outer channel wall and consequently, the complete droplet train leaves the disk via the first outlet channel. The forced contact of the droplets with the channel walls under the extreme “artificial gravity” of the centrifugal field is a new droplet handling operation supplementing our centrifugal multiphase-fluidics platform.

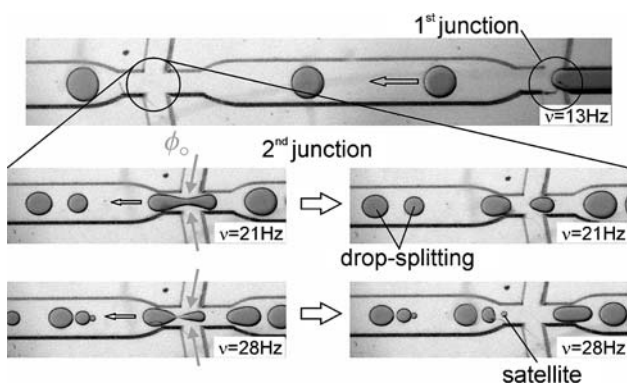
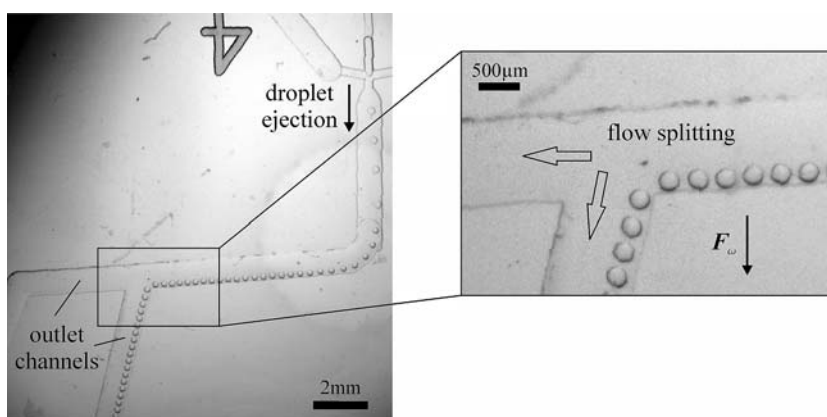


Fig. 10 Above a critical frequency, a droplet can be split at a second downstream junction. A further enlargement of the spinning frequency leads to the reproducible formation of a satellite droplet

Fig. 11 Water droplets sediment within an oil stream towards the outer wall of a nearly azimuthal channel. The droplets are consequently deflected into the first outlet channel at the split-intersection



4.4 Two-phase droplets

We produce two-phase droplets by enclosing two phases which are commonly guided to the junction of the flow-focusing structure into one droplet (Fig. 12). A structure to produce such two-phase droplets has been realized and tested with pure water and ink as the two phases to be enclosed in the droplet. The two dispersed phases are contacted in the central inlet channel prior to their injection into the junction of the flow focusing structure.

Bi-colored droplets break off at the junction and emerge into the outlet channel. The contacting and parallel flow of the two liquids in the central channel displayed tendencies to become unstable, e.g. by the displacement of one liquid by the other within the experiments, eventually leading to single-phase droplets. Thus, further improved structures are to be fabricated in the future to get more stable hydrodynamics at the junction.

The double-droplet capability opens several new areas of application. For example, regarding miscible liquids, mixing experiments within very small “reaction chambers” represented by the droplets can be accom-

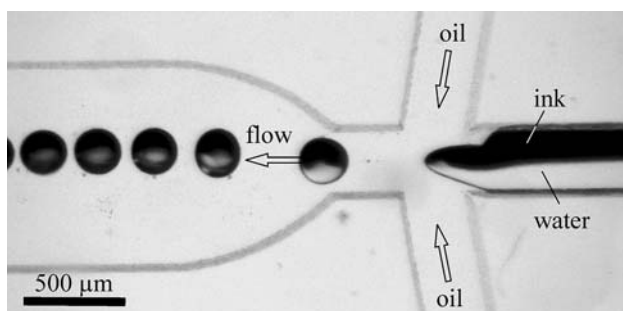


Fig. 12 Two miscible liquids (ink and pure water) are contacted within a microchannel. At the junction, a sequence monodisperse two colored droplets break off in the continuous oil flow

plished (Song et al. 2003; Roach et al. 2005; Gunther et al. 2005; Zheng et al. 2003). Another application is the production of two-colored droplets followed by a polymerization step to fabricate bi-colored beads, e.g., for display technologies (Nisisako et al. 2004a, b).

5 Conclusion

Novel centrifugal microfluidic methods for the continuous production and manipulation of highly monodisperse trains of water droplets in an oil flow have been investigated. By changing the channel geometry and the frequency of rotation, the flow regime could be switched between monodisperse emulsions and segmented-flow and the droplet size and generation rate can be influenced. Key unit operations such as splitting of droplets, separation of droplets from the continuous phase, and the production of two-phase droplets are demonstrated.

We expect further benefits of porting multiphase flows to the centrifugal platform in the comparatively high discharge rates (Ducrée et al. 2004) as well as the facile integration of centrifugal droplet sedimentation, thus enabling novel applications in the fields of droplet-based analytics and microprocess engineering.

Acknowledgements The authors are grateful to the partial support by the German “Landesstiftung Baden-Württemberg gGmbH”.

References

- Anna SL, Bontoux N, Stone HA (2003) Formation of dispersions using “flow focusing” in microchannels. *Appl Phys Lett* 82(3):364–366
- Brenner T, Glatzel T, Zengerle R, Ducrée J (2005) Frequency-dependent transversal flow control in centrifugal microfluidics. *Lab Chip* 5(2):146–150

- Cramer C, Fischer P, Windhab EJ (2004) Drop formation in a co-flowing ambient fluid. *Chem Eng Sci* 59(15):3045–3058
- Dendukuri D, Tsoi K, Hatton TA, Doyle PS (2005) Controlled synthesis of nonspherical microparticles using microfluidics. *Langmuir* 21(6):2113–2116
- Ducrée J, Schlosser HP, Haerberle S, Glatzel T, Brenner T, Zengerle R (2004) Centrifugal platform for high-throughput reactive micromixing. In: Laurell T, Nilsson J, Jensen KF, Harrison DJ, Kutter JP (eds) *Proceedings of μ TAS 2004*, 8th International Conference on Miniaturized Systems for Chemistry and Life Sciences, September 26–30, Malmö, Sweden, pp 554–556
- Ducrée J, Haerberle S, Brenner T, Glatzel T, Zengerle R (2005) Patterning of flow and mixing in rotating radial microchannels. *Microfluid Nanofluid* 2(2):97–105
- Ducrée J, Brenner T, Haerberle S, Glatzel T, Zengerle R (2006) Multilamination of flows in planar networks of rotating microchannels. *Microfluid Nanofluid* 2(1):78–84
- Ganan-Calvo AM, Gordillo JM (2001) Perfectly monodisperse microbubbling by capillary flow focusing. *Phys Rev Lett* 87(27):274501
- Garstecki P, Gitlin I, DiLuzio W, Whitesides GM, Kumacheva E, Stone HA (2004) Formation of monodisperse bubbles in a microfluidic flow-focusing device. *Appl Phys Lett* 85(13):2649–2651
- Garstecki P, Stone HA, Whitesides GM (2005) Mechanism for flow-rate controlled breakup in confined geometries: a route to monodisperse emulsions. *Phys Rev Lett* 94(16):164501
- Geschke O, Klank H, Telleman P (2004) *Microsystem engineering of lab-on-a-chip devices*. Wiley, Weinheim
- Grumann M, Brenner T, Beer C, Zengerle R, Ducrée J (2005) Visualization of flow patterning in high-speed centrifugal microfluidics. *Rev Sci Instrum* 76(2):025101
- Gunther A, Jhunjhunwala M, Thalmann M, Schmidt MA, Jensen KF (2005) Micromixing of miscible liquids in segmented gas–liquid flow. *Langmuir* 21(4):1547–1555
- Haerberle S, Brenner T, Schlosser HP, Zengerle R, Ducrée J (2005a) Centrifugal micromixer. *Chem Eng Technol* 28(5):613–616
- Haerberle S, Zengerle R, Ducrée J (2005b) Online process control for centrifugal microfluidics. In: *Proceedings of Transducers 05, the 13th International Conference on Solid-State Sensors, Actuators and Microsystems*, June 5–9, Seoul, Korea, pp 1525–1528
- Haerberle S, Schlosser HP, Zengerle R, Ducrée J (2005c) A centrifuge-based microreactor. In: *IMRET 8, 8th International Conference on Microreaction Technology*, April 10–14, Atlanta, USA, p TK-129f
- Haerberle S, Zengerle R, Ducrée J (2005d) Monodisperse droplet trains and segmented flow for centrifugal microfluidics. In: *Proceedings 9th International Conference on Miniaturized Systems for Chemistry and Life Sciences (μ TAS 2005)*, Boston, USA, pp 635–637
- Haerberle S, Schmitt N, Zengerle R, Ducrée J (2006) A centrifuge-magnetically actuated gas micropump. In: *Proceedings of 19th International Conference on Microelectro Mechanical Systems (MEMS 2006)*, Istanbul, Turkey, pp 166–169
- Hessel V, Lowe H, Stange T (2002) Microchemical processing at IMM—from pioneering work to customer-specific services. *Lab Chip* 2(1):14N–21N
- Joanicot M, Ajdari A (2005) Droplet control for microfluidics. *Science* 309(5736):887–888
- Kim DS, Kwon TH (2006) Modeling, analysis and design of centrifugal force-driven transient filling flow into a circular microchannel. *Microfluid Nanofluid* 2(2):125–140
- Link DR, Anna SL, Weitz DA, Stone HA (2004) Geometrically mediated breakup of drops in microfluidic devices. *Phys Rev Lett* 92(5):054503
- Lord Rayleigh FRS (1878) On the instability of jets. *Proc Lond Math Soc* 10(4):4–13
- Nisisako T, Torii T, Higuchi T (2004a) Novel microreactors for functional polymer beads. *Chem Eng J* 101(1–3):23–29
- Nisisako T, Torii T, Higuchi T (2004b) Controlled production of functional polymeric microspheres using multi-phase microfluidics. In: Laurell T, Nilsson J, Jensen KF, Harrison DJ, Kutter JP (eds) *Proceedings of μ TAS 2004*, 8th International Conference on Miniaturized Systems for Chemistry and Life Sciences, September 26–30, Malmö, Sweden, pp 408–410
- Roach LS, Song H, Ismagilov RF (2005) Controlling nonspecific protein adsorption in a plug-based microfluidic system by controlling interfacial chemistry using fluorophilic surfactants. *Anal Chem* 77(3):785–796
- Shestopalov IA, Tice JD, Ismagilov RF (2004) Multi-step chemical reactions performed on millisecond time scale in a microfluidic droplet-based system. *Lab Chip* 4:316–321
- Song H, Bringer MR, Tice JD, Gerds CJ, Ismagilov RF (2003) Experimental test of scaling of mixing by chaotic advection in droplets moving through microfluidic channels. *Appl Phys Lett* 83(22):4664–4666
- Sugiura S, Nakajima M, Iwamoto S, Seki M (2001) Interfacial tension driven monodispersed droplet formation from microfabricated channel array. *Langmuir* 17(18):5562–5566
- Tan YC, Fisher JS, Lee AI, Cristini V, Lee AP (2004) Design of microfluidic channel geometries for the control of droplet volume, chemical concentration, and sorting. *Lab Chip* 4(4):292–298
- Thorsen T, Roberts RW, Arnold FH, Quake SR (2001) Dynamic pattern formation in a vesicle-generating microfluidic device. *Phys Rev Lett* 86(18):4163–4166
- Utada AS, Lorenceau E, Link DR, Kaplan PD, Stone HA, Weitz DA (2005) Monodisperse double emulsions generated from a microcapillary device. *Science* 308(5721):537–541
- Windhab EJ, Dressler M, Feigl K, Fischer P, Megias-Alguacil D (2005) Emulsion processing—from single-drop deformation to design of complex processes and products. *Chem Eng Sci* 60(8–9):2101–2113
- Zheng B, Roach LS, Ismagilov RF (2003) Screening of protein crystallization conditions on a microfluidic chip using nanoliter-size droplets. *J Am Chem Soc* 125(37):11170–11171